Supporting Information

Molecular Origin of the Odd-Even Effect of Macroscopic Properties of *n*-Alkanethiolate Self-Assembled Monolayers: Bulk or Interface?

Fadwa Ben Amara[‡], *Eric R. Dionne*[‡], *Sahar Kassir, Christian Pellerin*, and Antonella Badia**

Département de chimie, FRQNT Quebec Centre for Advanced Materials, Université de Montréal, C.P. 6128, succursale Centre-ville, Montréal, QC H3C 3J7 CANADA

Table of Contents

1. EXPERIMENTAL SECTION

Materials. The following *n*-alkanethiols and reagents were purchased and used without further purification: 1-heptanethiol ($CH_3(CH_2)_6SH$, 98%, Alfa Aesar), 1-octanethiol ($CH_3(CH_2)_7SH$, 98%, Alfa Aesar), 1-nonanethiol ($CH_3(CH_2)_8SH$, 98%, Alfa Aesar), 1-decanethiol ($CH_3(CH_2)_9SH$, 96%, Sigma-Aldrich), 1-undecanethiol ($CH_3(CH_2)_{10}SH$, 98%, Sigma-Aldrich), 1-dodecanethiol ($CH_3(CH_2)_{11}SH$, ≥ 97%, Fluka), 1-tetradecanethiol ($CH_3(CH_2)_{13}SH$, ≥ 98%, Fluka), 1-pentadecanethiol ($CH_3(CH_2)_{14}SH$, 98%, Sigma-Aldrich), 1-octadecanethiol ($CH_3(CH_2)_{17}SH$, 98% Sigma-Aldrich), 1-dodecane-d_{25}-thiol ($CD_3(CD_2)_{11}SH$, 98 atom% D, CDN Isotopes), 1-bromotridecane (98%, Sigma-Aldrich), 1-bromoheptadecane (> 95%, Sigma-Aldrich), 1-bromononadecane (97%, Sigma-Aldrich), 1-eicosanol (98%, Sigma-Aldrich), sodium perchlorate (≥ 98%, Sigma-Aldrich), sodium methyl sulfate ($NaCH_3SO_4$, 99%, Acros), hydrogen peroxide 30% (A&C Ltd), ammonium hydroxide 28-30% (A&C Ltd), hydrochloric acid (reagent grade, A&C Ltd), and nitric acid (reagent grade, A&C Ltd). 1-Hexadecanethiol ($CH_3(CH_2)_{15}SH$, > 95%, Sigma-Aldrich) was purified by column chromatography (see details below). 1-Tridecanethiol ($CH_3(CH_2)_{12}SH$), 1-heptadecanethiol ($CH_3(CH_2)_{16}SH$), and 1-nonadecanethiol ($CH_3(CH_2)_{18}SH$) were synthesized by conversion of the corresponding aliphatic bromide to the alkanethiol (Scheme S1). 1-Eicosanethiol ($CH_3(CH_2)_{19}SH$) was synthesized from the corresponding aliphatic alcohol. Ultrapure water with a resistivity of 18.2 MΩ cm and total organic carbon of ≤ 5 ppb (MilliQ Gradient) was used to prepare the electrolyte solutions.

Purification of 1-hexadecanethiol. The commercially-available compound was purified prior to use by column chromatography (SiO_2, hexane:pentane (1:1v/v), $R_f = 0.75$) because it comprised a mixture of solid and liquid phases at room temperature. The purified product was a liquid.

Synthesis of 1-Bromoeicosane (1). 1-Eicosanol (0.980g, 3.28 mmol) was added to a mixture of 50 mL of 48% HBr and 100μL of concentrated H_2SO_4. The mixture was refluxed for 8 h. The HBr mixture was diluted with 25 mL of distilled water and 50 mL of hexanes was added with stirring. The hexanes phase was separated from the aqueous HBr phase and the HBr phase was further extracted with 2 × 50 mL of hexanes. The combined hexanes phases were washed twice with 75 mL of water, dried over anhydrous $MgSO_4$, filtered, and concentrated under reduced pressure. The crude product was purified by column chromatography (SiO_2, *n*-hexane) to yield 0.974 g (84%) of 1-bromoeicosane.

Synthesis of $CH_3(CH_2)_nSH$, *n* = 12, 16, 18, and 19. The syntheses of 1-tridecanethiol, 1-heptadecanethiol, 1-nonadecanethiol, and 1-eicosanthiol were performed in two steps using the appropriate 1-alkylbromide (**1**) as the starting material (Scheme S1).

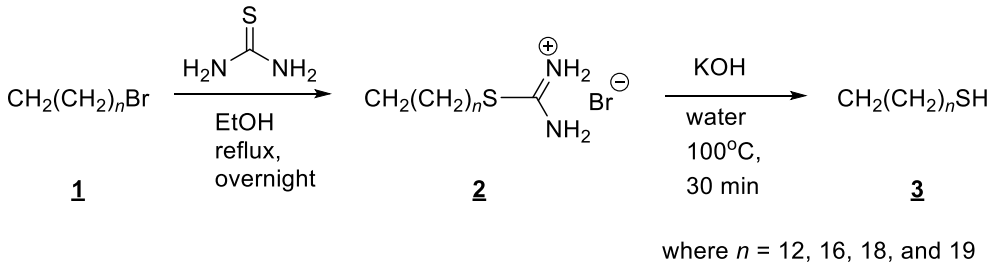

Scheme S1: Synthesis of $CH_3(CH_2)_nSH$, *n* = 12, 16, 18, and 19.

*Synthesis of the alkylisothiuronium bromide (**2**).* To a solution of 0.15 M of the alkylbromide (**1**) (1 eq) in ethanol, thiourea (2 eq) was added. The solution was thoroughly degassed and then placed in an oil bath and heated at reflux for 18 h. After cooling to room temperature, the solvent was removed under reduced pressure. Hexane was added to the residue (to dissolve the unreacted starting material), and the suspension was stirred for 30 min. The solids were then removed by filtration to give compound **2** quantitatively. This product was used in the next step without further purification.

Synthesis of the n-alkanethiol (**3**). A degassed aq. 0.2 M solution of the alkylisothiuronium bromide (**2**) (1 eq) to which KOH (1.2 eq) was added, was heated at 100 ºC for 30 min. The solution was cooled at room temperature, acidified with 1 M aq. HCl, and extracted with dichloromethane. The combined halogenated layers were dried over $MgSO_4$, filtered, and concentrated under reduced pressure. The crude product was purified by column chromatography (SiO_2, hexanes), giving the pure product as a white powder.

1-tridecanethiol (*n* = 12) (41.2%, R_f = 0.68)
^{1}H NMR (500 MHz, $CDCl_3$) δ: 2.53 (q, 2H, $CH_3(CH_2)_{11}CH_2SH$); 1.61 (p, 2H, $CH_3(CH_2)_{10}CH_2CH_2SH$); 1.38 (p, 2H, $CH_3(CH_2)_9CH_2(CH_2)_2SH$); 1.33 (t, 1H, *J*=7.7 Hz, $CH_3(CH_2)_{11}CH_2SH$); 1.26 (s(broad), 18H, $CH_3(CH_2)_9CH_2(CH_2)_2SH$); 0.89 (t, 3H, *J*=7.0 Hz,$CH_3(CH_2)_{11}CH_2SH$).
^{13}C NMR (126 MHz, $CDCl_3$) δ: 34.07, 31.93, 29.68, 29.65, 29.60, 29.53, 29.36, 29.09, 28.40, 24.67, 22.70, 14.13.

1-heptadecanethiol (*n* = 16) (67.7%, R_f = 0.55)
^{1}H NMR (500 MHz, $CDCl_3$) δ: 2.54 (q, 2H, $CH_3(CH_2)_{15}CH_2SH$); 1.61 (p, 2H, $CH_3(CH_2)_{14}CH_2CH_2SH$); 1.37 (p, 2H, $CH_3(CH_2)_{14}CH_2CH_2SH$); 1.35 (t, 1H, *J* = 7.7 Hz, $CH_3(CH_2)_{15}CH_2SH$); 1.26 (s(broad), 26H, $CH_3(CH_2)_{13}CH2(CH_2)_2SH$); 0.89 (t, 3H, *J*=7.0 Hz, $CH_3(CH_2)_{15}CH_2SH$).
^{13}C NMR (126 MHz, $CDCl_3$) δ: 34.07, 31.94, 29.70, 29.68, 29.67, 29.66, 29.60, 29.53, 29.37, 29.09, 28.40, 24.67, 22.70, 14.13.

1-nonadecanethiol (*n* = 18) (66.6%, R_f = 0.75)
^{1}H NMR (500 MHz, $CDCl_3$) δ: 2.53 (q, 2H, $CH_3(CH_2)_{17}CH_2SH$); 1.61 (p, 2H, $CH_3(CH_2)_{16}CH_2CH_2SH$); 1.38 (p, 2H, $CH_3(CH_2)_{15}CH_2(CH_2)_2SH$); 1.34 (t, 1H,$CH_3(CH_2)_{17}CH_2SH$); 1.26 (s(broad), 30H, $CH_3(CH_2)_{15}CH_2\,(CH_2)_2SH$); 0.89 (t, 3H,$CH_3(CH_2)_{17}CH_2SH$).

1-eicosanethiol (*n* = 19) (R_f = 0.70)
^{1}H NMR (500 MHz, $CDCl_3$) δ: 2.53 (q, 2H, $CH_3(CH_2)_{18}CH_2SH$); 1.61 (p, 2H,$CH_3(CH_2)_{17}CH_2CH_2SH$); 1.38 (p, 2H, $CH_3(CH_2)_{16}CH_2(CH_2)_2SH$); 1.34 (t, 1H,$CH_3(CH_2)_{18}CH_2SH$); 1.26 (s(broad), 32H, $CH_3(CH_2)_{16}CH_2(CH_2)_2SH$); 0.89 (t, 3H,$CH_3(CH_2)_{18}CH_2SH$).

Example of a ^{1}H NMR spectrum

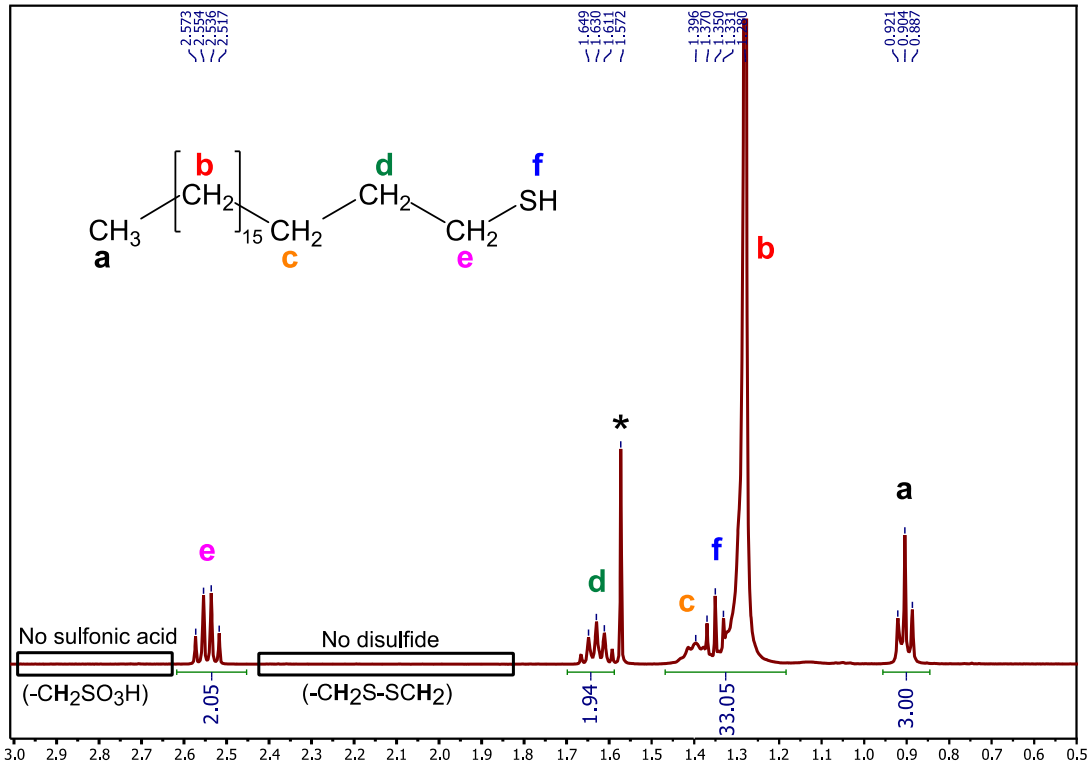

Preparation of $CH_3(CH_2)_nSAu$ SAMs for EIS. Gold bead electrodes were formed by bonding a 2–3 mm diameter gold granule (99.99%) to a 0.5 mm diameter gold wire (99.99%) with a butane torch. The surface areas of the gold beads were measured regularly by chronocoulometry using potassium ferricyanide as the redox probe, and ranged from 0.20 to 0.28 cm^2. Whether for a new gold bead or to recondition a used one, the gold bead electrodes were cleaned as follows. They were first sonicated in a 2:1 (v/v) mixture of NH_4OH/H_2O_2 for 60 min, rinsed copiously with ultrapure water, and subjected to a 15 min treatment in an oxygen-plasma cleaner at medium RF power setting (Harrick model PDC-32G). Prior to SAM formation, the gold bead was immersed in dilute aqua regia (3:1:6 $HCl/HNO_3/H_2O$) for ca. 10 min to dissolve away gold and surface impurities from the bead surface and remove surface impurities, rinsed copiously with ultrapure water, and sonicated in ultrapure water

for 2 min to remove traces of acid. Finally, the bead was flame-annealed and quenched in ultrapure water thrice and rinsed thoroughly with absolute ethanol. The bead was immersed in an ethanolic solution of 0.2 mM $CH_3(CH_2)_nSH$ for 18–24 h at room temperature in a sealed incubation vial. Prior to use, the SAM-modified bead electrode was removed from the $CH_3(CH_2)_nSH$ solution, rinsed copiously with absolute ethanol, followed by ultrapure water, and dried with nitrogen.

Preparation of $CH_3(CH_2)_nSAu$ SAMs for contact angle goniometry and IRRAS. Glass slides (B270, Esco Products) of 20 mm × 25 mm were first cleaned by immersion in a solution of 3:1 v/v concentrated H_2SO_4/30% H_2O_2 (Warning - piranha solution is a strong oxidizer. Handle with extreme caution!) at room temperature. The glass slides were rinsed copiously with ultrapure water, sonicated thrice in ultrapure water to completely remove traces of sulfuric acid, sonicated once in absolute ethanol, and dried under a stream of nitrogen gas.

A gold thin film was deposited on the clean glass slides by thermal evaporation using a VE-90 vacuum evaporator (Thermionics Vacuum Products) equipped with a 1 kVA resistive power supply, turbomolecular pump, and QCM thickness monitor. The chamber was evacuated to a base pressure of $\sim 3 \times 10^{-7}$ Torr. A 5 nm layer of titanium (99.99%) was first deposited onto the glass at a rate of 0.01 nm s^{-1}. The substrates were heated to ~200 ^oC with a UV lamp before the start of the gold evaporation. A 150 nm layer of gold (99.99%) was deposited in successive steps of progressively slower rate to promote the formation of larger grains while reducing the overall evaporation time[1-2]: 0–65 nm deposited at 0.1 nm s^{-1}, 65–80 nm deposited at 0.05 nm s^{-1}, 80–95 nm deposited at 0.03 nm s^{-1}, 95–110 nm deposited at 0.02 nm s^{-1}, 110–150 nm deposited at 0.01 nm s^{-1}. The substrate temperature was maintained between 200 ^oC and 240 ^oC during the gold deposition process by regulating the intensity of the UV lamp.

After cooling down to room temperature, the gold-coated glass slides were removed from the evaporator chamber and immediately immersed in ethanolic solutions of 0.2 mM $CH_3(CH_2)_nSH$. The gold substrates were incubated 16–24 h at room temperature in sealed incubation vials. Prior to measurements, the SAM-functionalized gold-coated slides were removed from the incubation solutions, thoroughly rinsed with pure ethanol followed by ultrapure water, and dried under nitrogen.

Electrochemical Impedance Spectroscopy (EIS). EIS measurements on the $CH_3(CH_2)_nSAu$ SAMs formed on gold bead electrodes were carried out using a three-electrode glass cell thermostatted with a circulation water bath and SP-200 potentiostat (BioLogic Science Instruments) equipped with an impedance analyzer. The electrolyte solution in the electrochemical cell (1.0 M $NaClO_4$ or 1.0 M $NaCH_3SO_4$) was deoxygenated by bubbling nitrogen for 20 min before the start of an experiment. Measurements were carried out under a blanket of argon at 22.0 ± 0.1 ^oC. Impedance spectra were acquired over a frequency span of seven decades, from 1 MHz to 1 Hz, at 32 points per decade using an ac voltage amplitude of 10 mV and an applied voltage of -0.185 V versus Ag/AgCl. The frequency spectra were transferred to the ZView software (version 3.4f, Scribner Associates) for complex nonlinear least-squares (CNLS) fitting to an appropriate electrical equivalent circuit.

SAM Capacitance Spectra. The electrochemical complex impedance $\hat{Z}(\omega)$ is generally represented as:

$$\hat{Z}(\omega) = Z_{Re}(\omega) + jZ_{Im}(\omega) \qquad \text{(S1)}$$

where Z_{Re} and Z_{Im} are the real and imaginary parts, j is the imaginary unit $(-1)^{1/2}$, and ω is the angular frequency of the applied ac potential perturbation (i.e., $\omega = 2\pi f$ where f is the applied frequency in Hz).

$\hat{Z}(\omega)$ is related phasorially to the complex capacitance $\hat{C}(\omega)$:[3-5]

$$\hat{C}(\omega) = \frac{1}{\hat{Z}(\omega)(j\omega)} \quad \text{(S2)}$$

and

$$\hat{C}(\omega) = C_{\mathrm{Re}}(\omega) + jC_{\mathrm{Im}}(\omega) \quad \text{(S3)}$$

where $C_{\mathrm{Re}}(\omega)$ and $C_{\mathrm{Im}}(\omega)$ are the real and imaginary components of $\hat{C}(\omega)$.

Capacitance spectra can be generated from Z_{Re} and Z_{Im} using the relations:[3, 5-6]

$$C_{\mathrm{Re}}(\omega) = -Z_{\mathrm{Im}}(\omega) / \omega|Z(\omega)|^2 \quad \text{(S4)}$$

$$C_{\mathrm{Im}}(\omega) = -Z_{\mathrm{Re}}(\omega) / \omega|Z(\omega)|^2 \quad \text{(S5)}$$

and

$$|Z(\omega)| = \sqrt{(Z_{\mathrm{Re}}(\omega))^2 + (Z_{\mathrm{Im}}(\omega))^2} \quad \text{(S6)}$$

Equivalent Electric Circuit Modeling of the Impedance Data. The impedance response of SAM-modified metal electrode was fit using the equivalent circuit R_s + CPE consisting of the solution resistance R_s in series with a constant phase element (CPE).[7-10] The use of a CPE in the place of a capacitor to model the interfacial capacitance significantly improves the quality of the fits of the experimental data. The CPE is a power law-dependent parameter that accounts for deviations from pure capacitor behavior. The impedance of a CPE $(Z_{\mathrm{CPE}}) = T^{-1}(j\omega)^{-\alpha}$, where T is the capacitance-type quantity whose units (F $s^{\alpha-1}$) depend on α and the CPE exponent α is the ideality factor ($0 < \alpha \leq 1$).[11] When $\alpha = 1$, the CPE is an ideal capacitor and $T = C$.

Contact Angle Goniometry. Static contact angle measurements were carried out using a homemade setup consisting of a micrometer syringe (Oakton Gilmont) to manually dispense a 2.0 μL droplet of probe liquid onto the SAM surface and a USB digital microscope to capture images of the liquid droplets on the surface. 8–10 droplets of ultrapure water were deposited on each SAM-modified gold-

coated slide. Images of the droplets were analyzed using the contact angle plugin of ImageJ (NIH) to determine the contact angle formed between the SAMs and water droplets.

Infrared Reflection Absorption Spectroscopy (IRRAS). Surface IR spectroscopy was carried out in specular reflection mode using a Tensor 27 FT-IR spectrometer (Bruker Optics) equipped with a liquid-nitrogen-cooled mercury-cadmium-telluride (MCT) detector and a specular reflection accessory (80Spec, Pike Technologies) purged with dry air. Spectra were collected at a grazing incidence angle of 80^{o} of the *p*-polarized light and 4 cm^{-1} resolution. Each spectrum is the average of 1024 scans. A spectrum of a perdeuterated SAM of $CD_3(CD_2)_{11}SAu$ served as the background. All peak positions and intensities were determined by fitting the spectra with the GRAMS/AI 7.00 software (Thermo Galactic).

2. ADDITIONAL RESULTS, STATISTICAL ANALYSES, AND CALCULATIONS

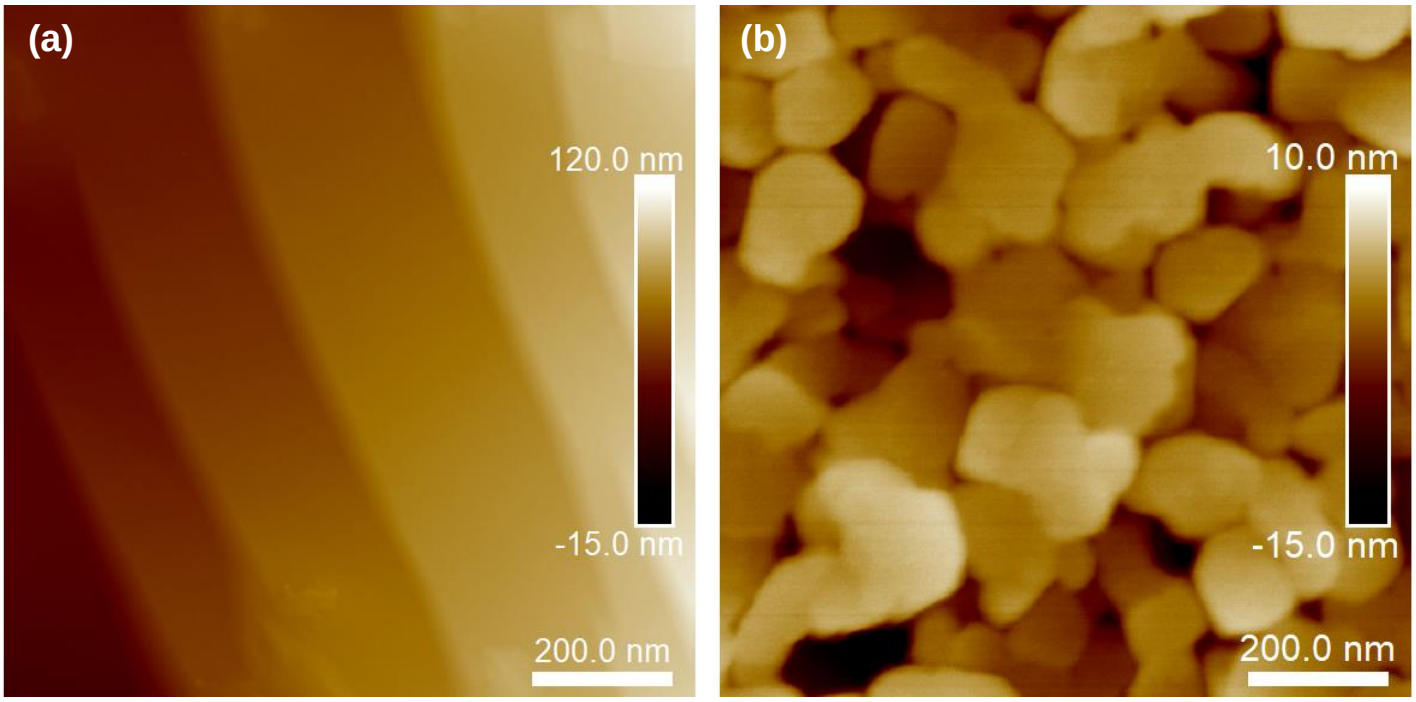

Figure S1. AFM height images (1 μm × 1 μm) of the (a) flame-annealed gold bead used for EIS and (b) thermally evaporated gold film on glass used for contact angle goniometry and IRRAS. The gold beads consist of large smooth strips, typically 100 to 300 nm in width and > 1 μm in length, of root-mean-square (rms) roughness < 0.2 nm separated by steps of heights of 8 to 15 nm. The surface of the thermally evaporated gold film comprises of flat gold grains of size of 167 ± 44 nm (N = 52 grains). The rms roughness over 1.0 μm^2 is 3 ± 1 nm. The rms roughness within the grains (area of 0.01 μm^2) of 0.5 ± 0.2 nm is comparable to that of ultraflat template-stripped gold.[12] The average grain sizes of the gold beads and films are at least 10 times larger than the typical molecular domain sizes of $CH_3(CH_2)_n$SAu SAMs formed at room temperature, which range from ~5 to ~15 nm.[13-15]

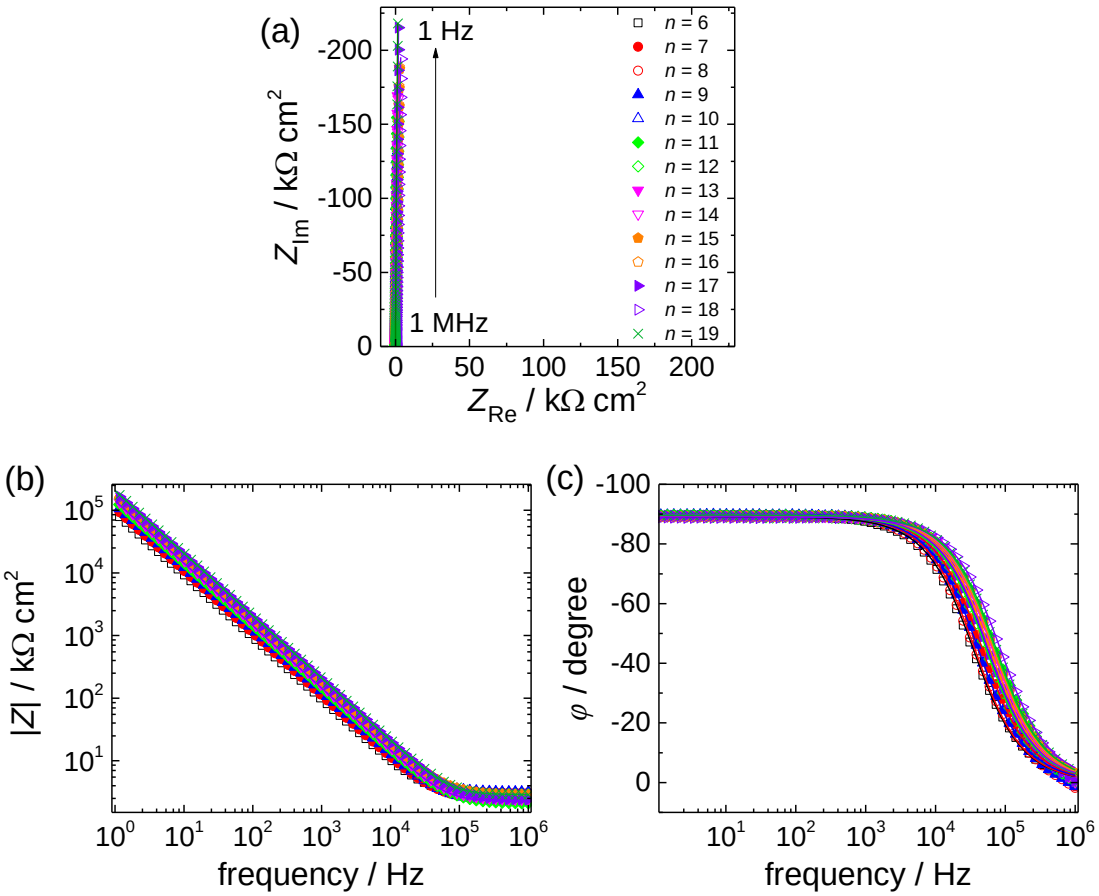

Figure S2. EIS data for $CH_3(CH_2)_nSAu$ SAMs of n = 6–19. (a) Complex plane plot of the imaginary Z_{Im} vs real Z_{Re} of the electrochemical impedance $\hat{Z}$. (b) Bode magnitude plot (impedance magnitude $|Z|$ vs frequency, where $|Z| = (Z_{Re}^2 + Z_{Im}^2)^{1/2}$). (c) Bode phase plot (phase angle φ vs frequency). Nonfaradaic impedance spectra were acquired at -0.185 V vs Ag/AgCl in 1.0 M $NaClO_{4(aq)}$. Symbols are the experimental data and solid lines are the results of the CNLS fits of the impedance data to the series equivalent circuit R_s + CPE.

Table S1. EIS of $CH_3(CH_2)_nSAu$ SAMs in 1.0 M $NaClO_{4(aq)}$. Results of CNLS fits of the impedance data to the equivalent circuit R_s + CPE. φ represents the phase angle shift of the ac potential perturbation at 1 Hz. R_s is the electrolyte solution resistance, T is the double-layer capacitance quantity of the constant phase element CPE, and α is the CPE exponent. The uncertainties are the 95% confidence intervals over N independent measurements.

n	$\varphi_{1\ Hz}$ / °	$R_s{}^a$ / Ω cm^2	α	T^a / μF cm^{-2} s$^{\alpha-1}$	N
6	89.2 ± 0.2	2.9 ± 0.2	0.992 ± 0.002	1.73 ± 0.03	16
7	89.2 ± 0.2	2.5 ± 0.2	0.993 ± 0.001	1.49 ± 0.06	14
8	89.2 ± 0.2	2.9 ± 0.1	0.993 ± 0.001	1.48 ± 0.03	17
9	89.2 ± 0.2	3.1 ± 0.1	0.994 ± 0.001	1.30 ± 0.03	20
10	89.2 ± 0.2	2.7 ± 0.1	0.994 ± 0.002	1.30 ± 0.03	19
11	89.0 ± 0.3	2.5 ± 0.2	0.991 ± 0.003	1.14 ± 0.02	13
12	88.8 ± 0.4	2.9 ± 0.1	0.994 ± 0.002	1.16 ± 0.03	16
13	88.8 ± 0.5	2.6 ± 0.1	0.992 ± 0.003	1.04 ± 0.01	12
14	88.8 ± 0.3	2.8 ± 0.2	0.992 ± 0.002	1.05 ± 0.03	10
15	89.0 ± 0.2	2.6 ± 0.2	0.993 ± 0.001	0.96 ± 0.02	23
16	88.9 ± 0.3	3.0 ± 0.2	0.992 ± 0.002	0.97 ± 0.02	16
17	88.9 ± 0.3	2.9 ± 0.2	0.991 ± 0.002	0.87 ± 0.02	20
18	89.1 ± 0.2	2.8 ± 0.1	0.993 ± 0.002	0.89 ± 0.02	13
19	88.3 ± 0.4	3.1 ± 0.2	0.994 ± 0.001	0.81 ± 0.01	12

[a] R_s and T are normalized for the exposed electrode area.

Ionic Insulating Character of the $CH_3(CH_2)_nSAu$ SAMs

The high impedance magnitude ($|Z|$), of the order of 10^5 Ω cm^2, measured at 1 Hz (Figure S2b) attests to the highly insulating character (low ionic permeability) of the SAMs under the given experimental conditions.[7] Consistent with this conclusion are the phase angles of 88–89° measured between 1 kHz and 1 Hz (Figure S2c and Table S1). An ideal capacitor exhibits a phase angle of 90° at all frequencies. Current leakage through the dielectric layer of the capacitor results in a deviation from 90°. We[16] and others[7] have shown that the most reliable indicator of the SAM leakiness is the measured phase angle at low frequency. Specifically, SAMs with a phase angle ≥ 88° at the characteristic frequencies for ion diffusion of 1–10 Hz can be considered, for practical purposes, to be free of defects, meaning that current leakage at monolayer defect sites is negligible.[7, 17] $CH_3(CH_2)_nSAu$ SAMs with phase angles < 88° at 1 Hz (i.e., "leaky" SAMs) were discarded. The impedance response of these SAMs could not be fit with an RC-type circuit.

We used a constant phase element (CPE) in the place of a capacitor in the series RC circuit (Figure 2a, inset) to model the interfacial capacitance as it significantly improves the quality of the fits of the experimental data. The CPE is a power law-dependent parameter that accounts for deviations from pure capacitor behavior. The impedance of a CPE (Z_{CPE}) = $T^{-1}(j\omega)^{-\alpha}$, where T is the capacitance-type quantity whose units (F $s^{\alpha-1}$) depend on α and the CPE exponent α is the ideality factor ($0 < \alpha \leq 1$).[11] When $\alpha = 1$, the CPE is an ideal capacitor and $T = C$. In practice, a deviation from unity (e.g., $0.85 < \alpha < 1$) is almost always observed, even for a near-perfect blocking film, due to the surface roughness and polycrystallinity of the underlying solid electrode.[7, 18] The CPE parameter T (Table S1), obtained from fits of the impedance data to the series equivalent circuit R_s + CPE, was used as the capacitance, referred to as C, since the values of the CPE exponent α are very close to 1 (i.e., α = 0.991–0.994),

indicating that the SAM-modified gold interface behaves as a near ideal capacitor, and do not show any chain length or odd-even dependence.[7, 9, 17, 19-20]

The measured capacitance is approximated by two capacitors in series:

$$C^{-1} = C_{SAM}^{-1} + C_D^{-1} \quad \text{(S7)}$$

where C_{SAM} is the capacitance of the SAM and C_D is the concentration-dependent diffuse layer capacitance of the electrolyte solution.[4, 8, 21-22] For densely-packed SAMs, C_D is at least an order of magnitude larger than C_{SAM} so that its contribution to the total capacitance can be neglected, as demonstrated experimentally by some studies.[8, 21]

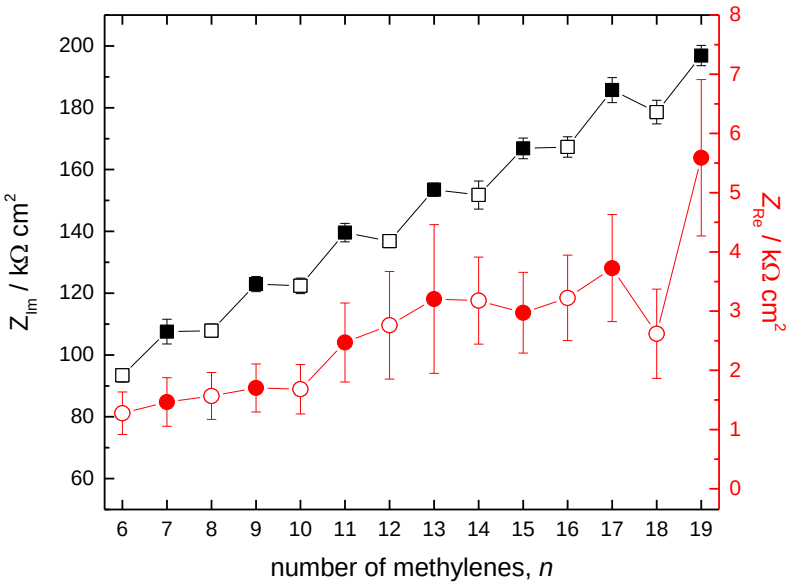

Figure S3. The real Z_{Re} and imaginary Z_{im} parts of the complex impedance $\hat{Z}$ vs n. Z_{Re} indicates the resistance of the SAM interface to current flow. Z_{im}, referred to as the reactance, describes the opposition of the SAM interface to changes in the current flow. Z_{im}, from which C_{Re} is derived (eq S4), shows an odd-even variation. Z_{Re} does not show a parity effect.

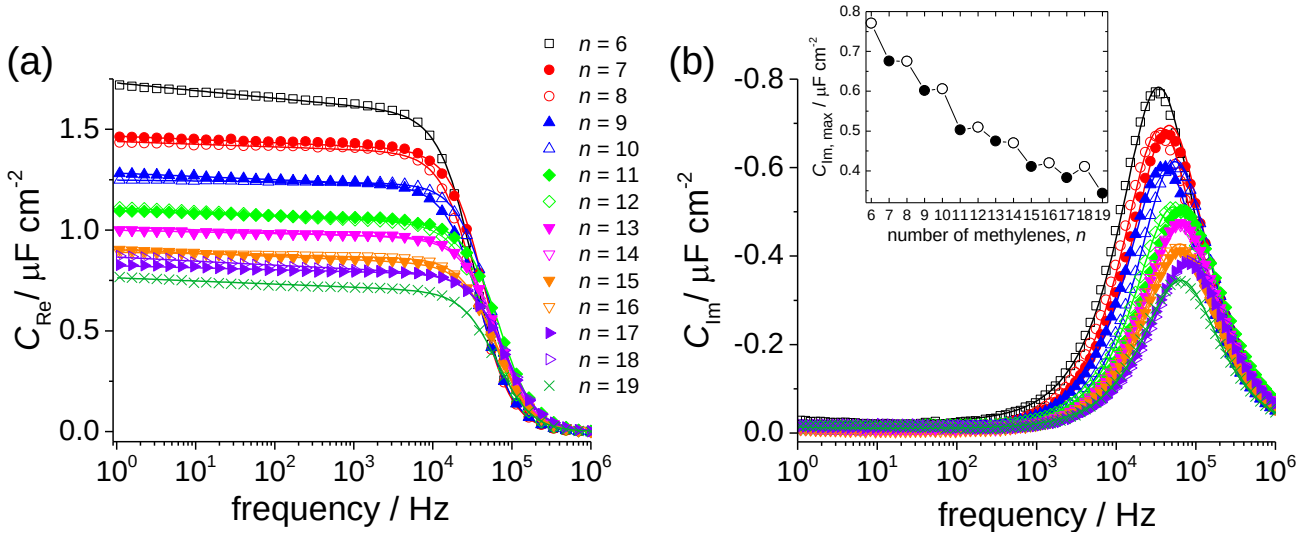

Figure S4. (a) Bode plot of the real component C_{Re} vs frequency. (b) Bode plot of the imaginary component C_{Im} vs frequency. Inset: C_{Im} value at the peak maximum vs n. The peak C_{Im} is approximately equal to one-half of the C_{Re} value at low frequency, indicative of a near homogeneous dielectric relaxation, and thus exhibits an odd-even variation.[6] Lines in the inset are a guide to the eye. Symbols are the experimental data and solid lines are the results of CNLS fits of the impedance data to the series equivalent circuit R_s + CPE.

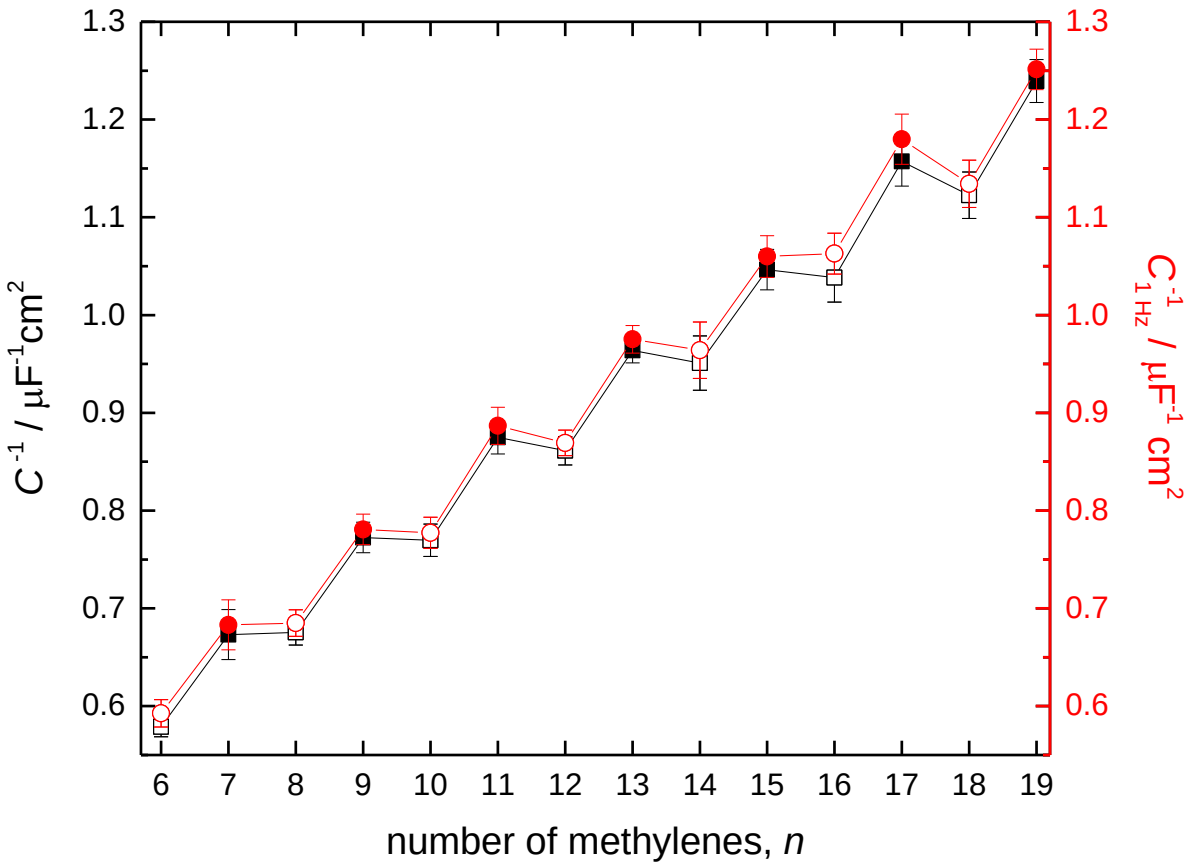

Figure S5. Reciprocal of the capacitance as a function of *n*: fitted *T* values (Table S1), C^{-1}, or C_{Re} at 1 Hz, $C_{1\,Hz}^{-1}$.

Comparison of Fitted Parameters Obtained from the Helmholtz and Randles Equivalent Circuits

Figure S6. Comparison of the parameters obtained from fits of the impedance data to the equivalent circuits R_s + CPE (Helmholtz) and R_s + R_{SAM}‖CPE (Randles) for selected chain lengths. The Helmholtz circuit describes ion-blocking SAMs,[7-10] while the Randles circuit is used to fit the impedance response of SAMs presenting sites for ion permeation[19-21, 23]. The equivalent circuit used for each fitting is framed in red. R_p in the fitting software is R_{SAM}. (a) n = 7, (b) n = 8, (c) n = 11, (d) n = 12, (e) n = 17, and (f) n = 18.

(a) $CH_3(CH_2)_7SAu$ (n = 7)

R_s + CPE:

$R_s = 2.44 \pm 0.01\ \Omega\ cm^2$

$T = 1.50 \times 10^{-6} \pm 7.29 \times 10^{-9}\ F\ cm^{-2}\ s^{\alpha-1}$

R_s + R_{SAM}‖CPE:

$R_s = 2.44 \pm 0.01\ \Omega\ cm^2$

$T = 1.50 \times 10^{-6} \pm 7.30 \times 10^{-9}\ F\ cm^{-2}\ s^{\alpha-1}$

$R_{SAM} = 8.13 \times 10^{12} \pm 1.59 \times 10^{18}\ \Omega\ cm^2$

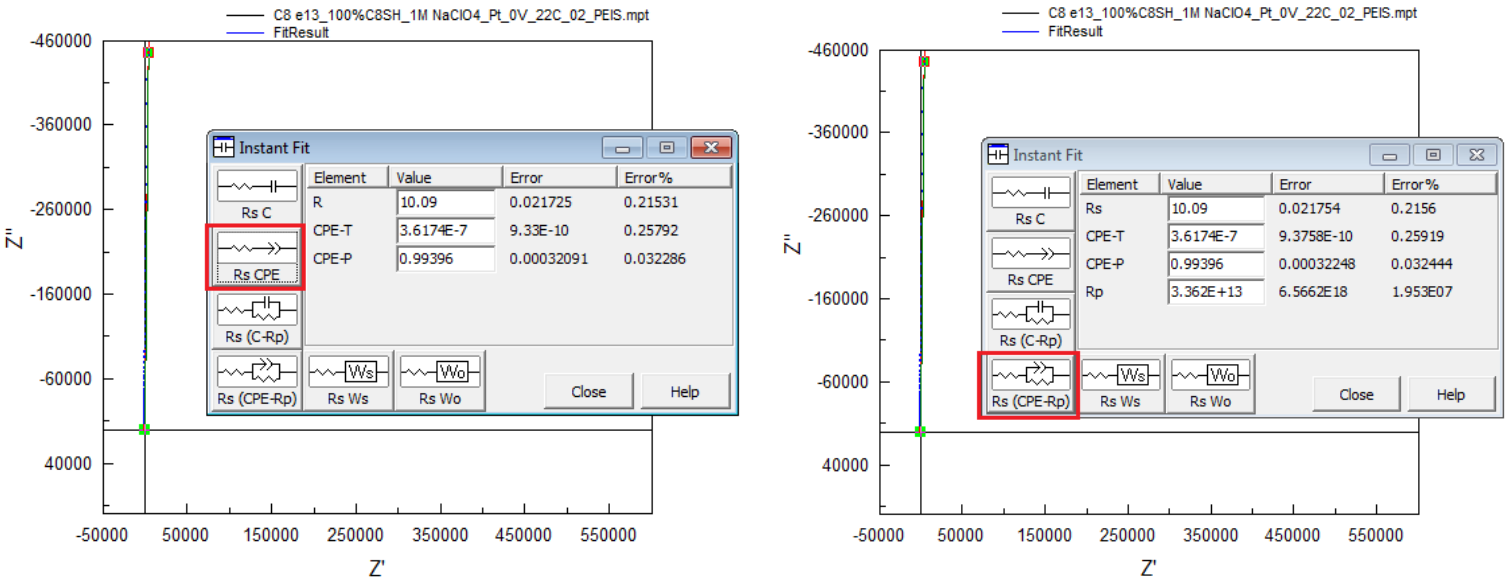

(b) $CH_3(CH_2)_8SAu$ (n = 8)

R_s + CPE:

$R_s = 3.16 \pm 0.01\ \Omega\ cm^2$

$T = 1.46 \times 10^{-6} \pm 6.76 \times 10^{-9}\ F\ cm^{-2}\ s^{\alpha-1}$

R_s + R_{SAM}‖CPE:

$R_s = 3.16 \pm 0.01\ \Omega\ cm^2$

$T = 1.46 \times 10^{-6} \pm 6.77 \times 10^{-9}\ F\ cm^{-2}\ s^{\alpha-1}$

$R_{SAM} = 4.38 \times 10^{12} \pm 5.64 \times 10^{17}\ \Omega\ cm^2$

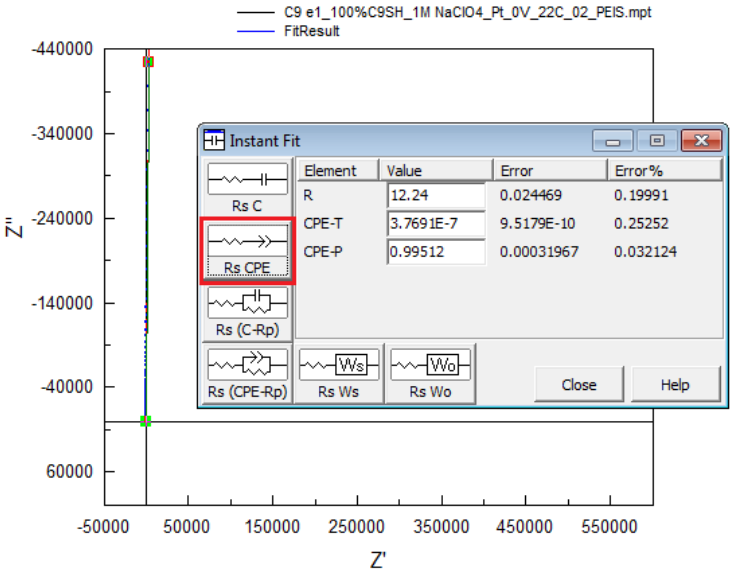

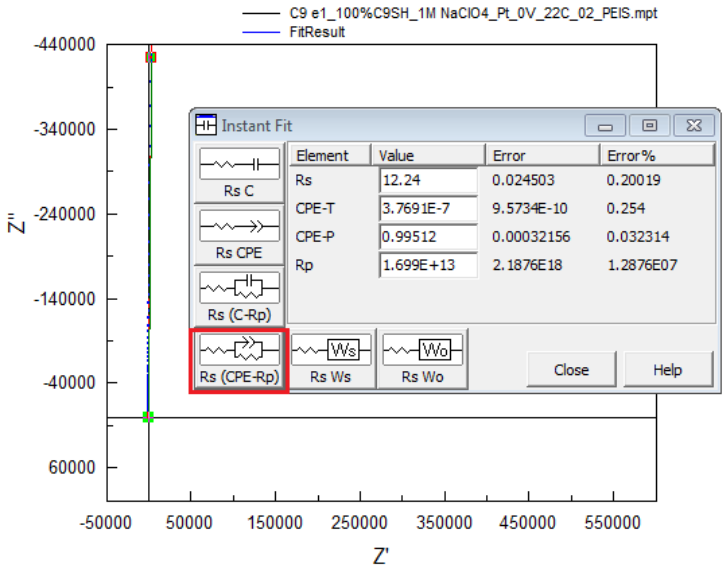

(c) $CH_3(CH_2)_{11}SAu$ (n = 11)

R_s + CPE:

$R_s = 2.17 \pm 0.01\ \Omega\ cm^2$

$T = 1.11 \times 10^{-6} \pm 5.57 \times 10^{-9}\ F\ cm^{-2}\ s^{\alpha-1}$

R_s + R_{SAM}‖CPE:

$R_s = 2.17 \pm 0.01\ \Omega\ cm^2$

$T = 1.11 \times 10^{-6} \pm 5.58 \times 10^{-9}\ F\ cm^{-2}\ s^{\alpha-1}$

$R_{SAM} = 1.38 \times 10^{13} \pm 1.76 \times 10^{18}\ \Omega\ cm^2$

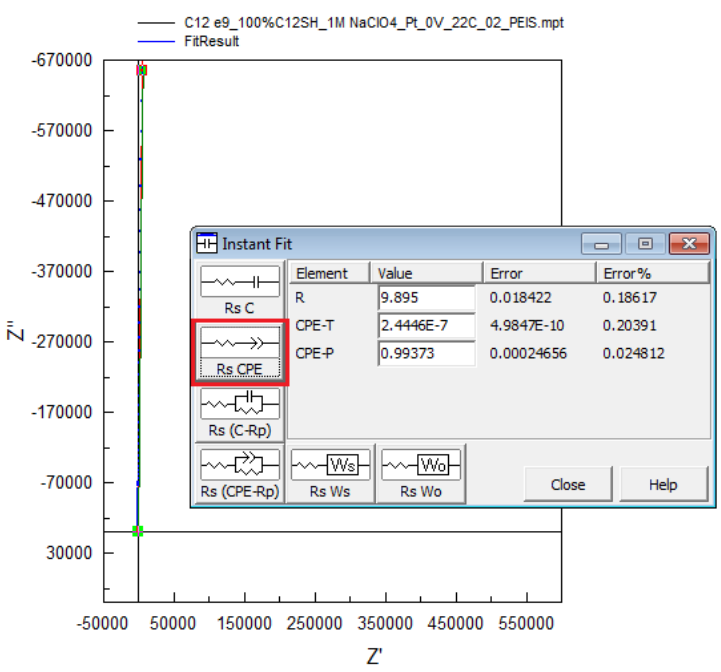

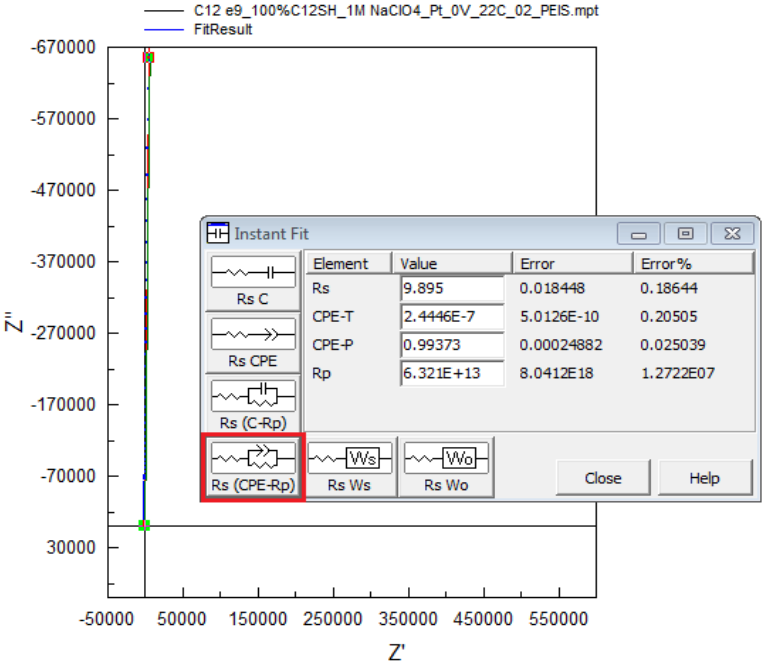

(d) $CH_3(CH_2)_{12}SAu$ (n = 12)

R_s + CPE:

$R_s = 3.04 \pm 0.01\ \Omega\ cm^2$

$T = 1.13 \times 10^{-6} \pm 4.46 \times 10^{-9}\ F\ cm^{-2}\ s^{\alpha-1}$

R_s + R_{SAM}‖CPE:

$R_s = 2.91 \pm 0.01\ \Omega\ cm^2$

$T = 1.13 \times 10^{-6} \pm 4.47 \times 10^{-9}\ F\ cm^{-2}\ s^{\alpha-1}$

$R_{SAM} = 5.55 \times 10^{8} \pm 6.82 \times 10^{9}\ \Omega\ cm^2$

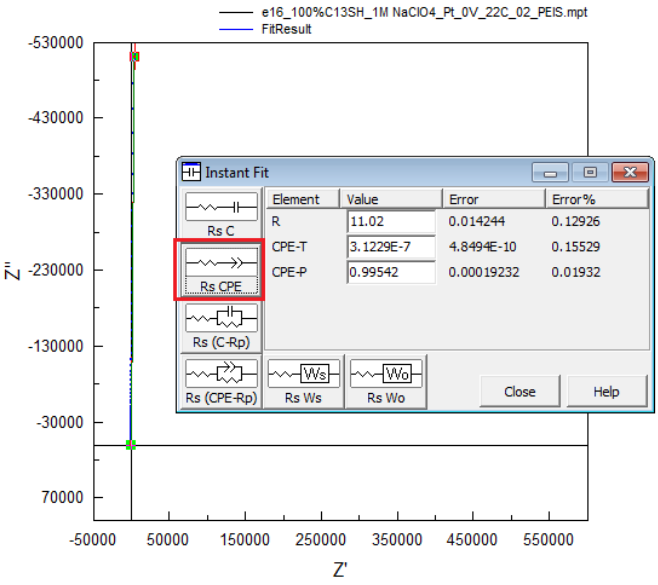

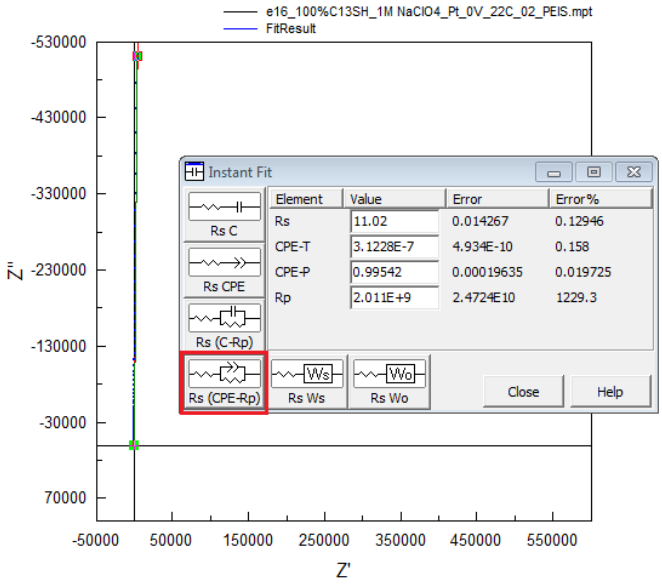

(e) $CH_3(CH_2)_{17}SAu$ (n = 17)

R_s + CPE:

$R_s = 3.80 \pm 0.01\ \Omega\ cm^2$

$T = 7.93 \times 10^{-7} \pm 3.09 \times 10^{-9}\ F\ cm^{-2}\ s^{\alpha-1}$

R_s + R_{SAM}‖CPE:

$R_s = 3.80 \pm 0.01\ \Omega\ cm^2$

$T = 7.93 \times 10^{-7} \pm 3.10 \times 10^{-9}\ F\ cm^{-2}\ s^{\alpha-1}$

$R_{SAM} = 1.23 \times 10^{8} \pm 2.16 \times 10^{8}\ \Omega\ cm^2$

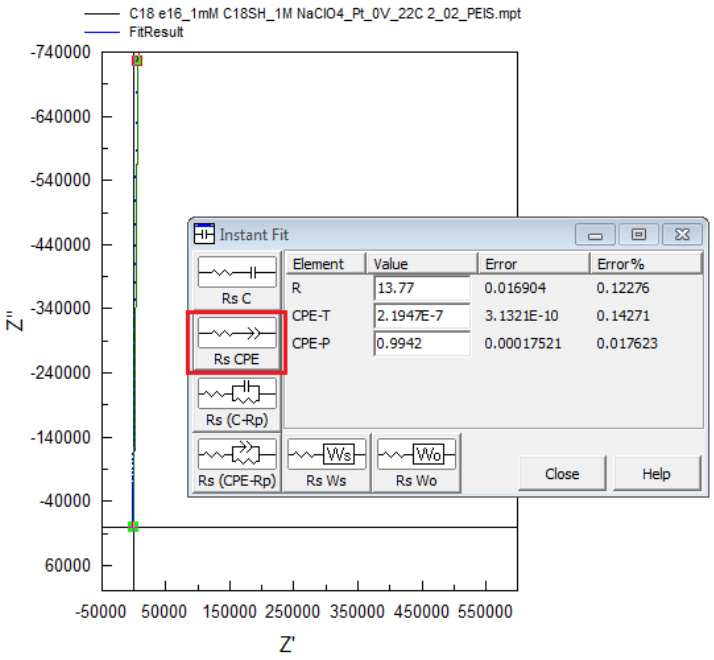

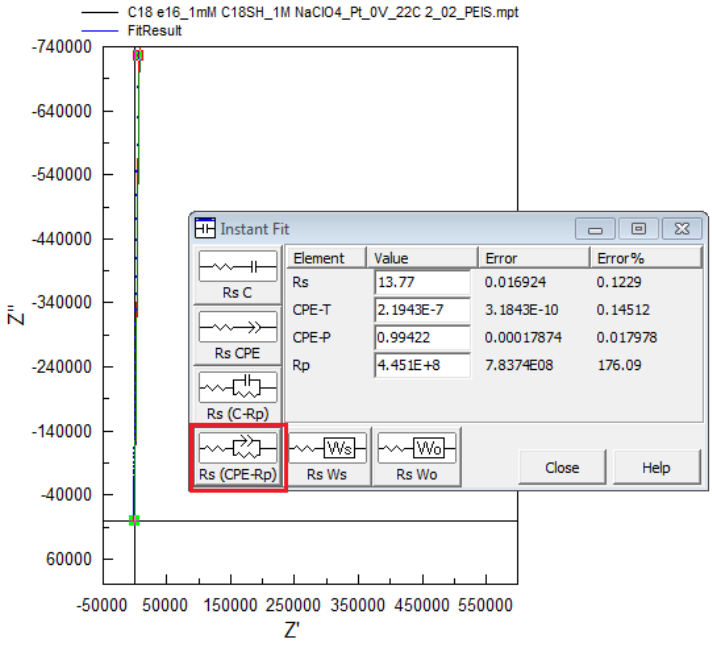

(f) $CH_3(CH_2)_{18}SAu$ (n = 18)

R_s + CPE:

$R_s = 2.25 \pm 0.02\ \Omega\ cm^2$

$T = 1.13 \times 10^{-6} \pm 1.08 \times 10^{-8}\ F\ cm^{-2}\ s^{\alpha-1}$

R_s + R_{SAM}‖CPE:

$R_s = 2.25 \pm 0.02\ \Omega\ cm^2$

$T = 1.13 \times 10^{-6} \pm 1.08 \times 10^{-8}\ F\ cm^{-2}\ s^{\alpha-1}$

$R_{SAM} = 2.98 \times 10^{12} \pm 1.07 \times 10^{17}\ \Omega\ cm^2$

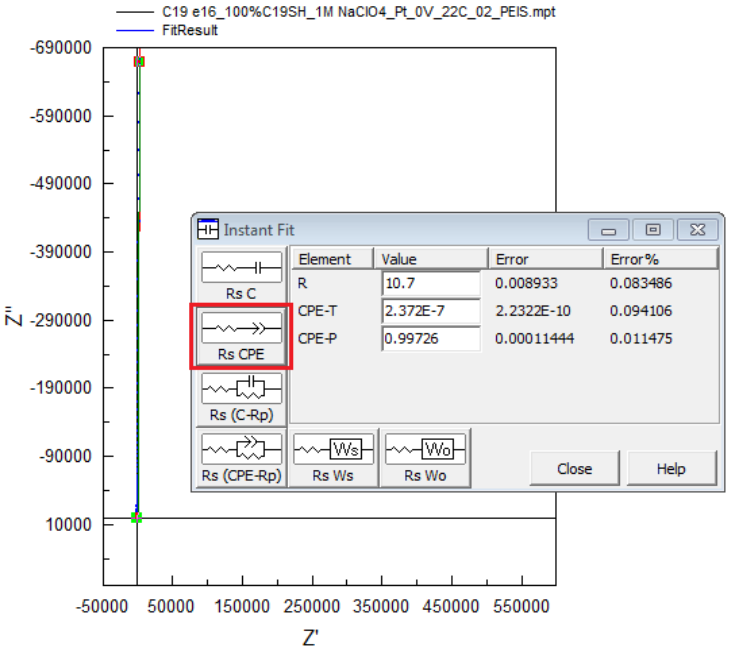

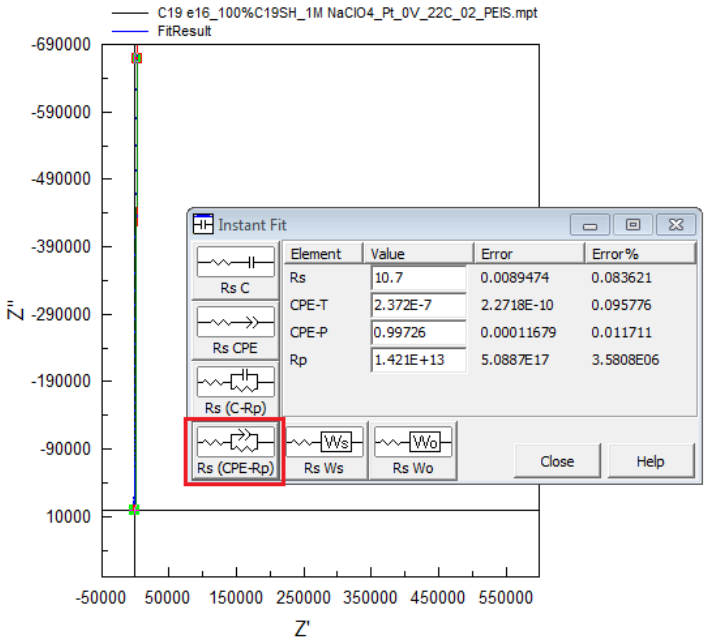

Statistical Analyses[24]

Two-Tailed *t*-Test Results (at 99% Confidence Level)

i. If $t_{calculated} > t_{Student}$, we conclude that the two means are not the same. The difference is significant.
ii. For any value of $P \leq 0.01$, we would reject the null hypothesis and conclude that the means are not the same.
iii. The pairs for which the means are statistically the same (cannot reject the null hypothesis) are highlighted in gray.
iv. For **Tables S2** and **S3**: *N* represents the number of independent measurements, $t_{calculated}$ is the calculated value of Student's *t*, $t_{Student}$ is the two-tailed Student's *t* value obtained from *t*-distribution tables at the degree of freedom df.
v. An *F*-test was performed prior to the two-tailed *t*-test calculation of a tested pair. If $F_{calculated} > F_{table}$, we can't reject the null hypothesis and the two-tailed *t*-test on the pair was done assuming equal variances. If $F_{calculated} < F_{table}$, the two-tailed *t*-test on the pair was done assuming unequal variances.

Table S2. Capacitance of the $CH_3(CH_2)_nSAu$ SAM.

n	$\bar{x}$ / μF cm^{-2}	*s* / μF cm^{-2}	*N*	Tested Pairs	P-value	$t_{calculated}$	$t_{Student}$	df
6	1.73	0.06	16	*n* = 6/7	2.96×10^{-8}	7.578	2.763	28
7	1.49	0.11	14	*n* = 7/8	0.744	0.330	2.756	29
8	1.48	0.06	17	*n* = 8/9	4.31×10^{-11}	9.388	2.724	35
9	1.30	0.06	20	*n* = 9/10	0.799	0.256	2.715	37
10	1.30	0.06	19	*n* = 10/11	1.01×10^{-8}	7.818	2.750	30
11	1.14	0.04	13	*n* = 11/12	0.244	1.190	2.771	27
12	1.16	0.04	16	*n* = 12/13	6.86×10^{-10}	9.446	2.779	26
13	1.04	0.02	12	*n* = 13/14	0.343	0.971	2.845	20
14	1.05	0.05	10	*n* = 14/15	6.81×10^{-6}	5.400	2.744	31
15	0.96	0.05	23	*n* = 15/16	0.624	0.494	2.715	37
16	0.97	0.05	16	*n* = 16/17	1.80×10^{-7}	6.527	2.728	34
17	0.87	0.04	20	*n* = 17/18	0.085	1.781	2.744	31
18	0.89	0.04	13	*n* = 18/19	7.39×10^{-7}	6.723	2.807	23
19	0.81	0.03	12					

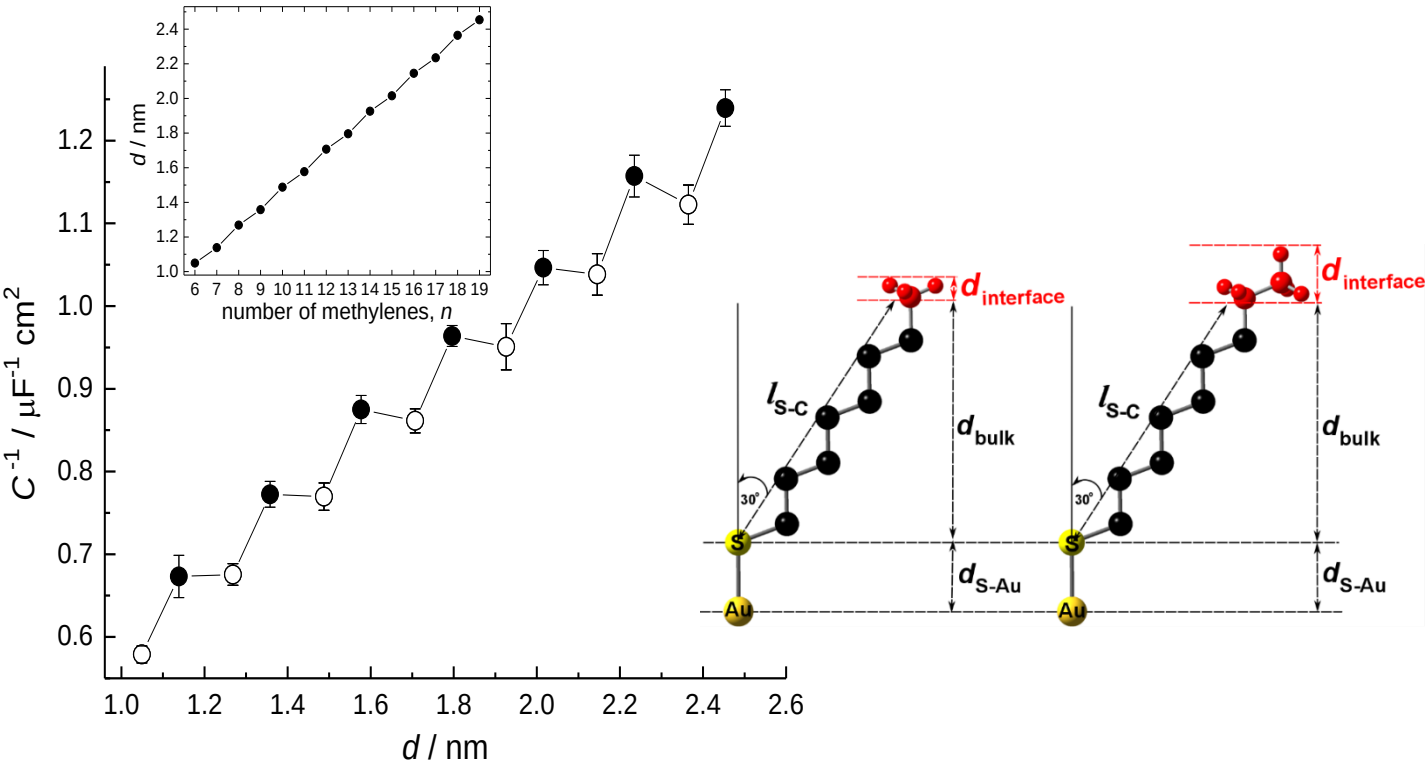

Figure S7. Reciprocal of the capacitance, C^{-1}, vs the SAM film thickness d calculated for n_{even} (d_{even}) and n_{odd} (d_{odd}) assuming a 30° tilt from the surface normal of all-trans extended alkyl chains:

$$d_{even} = d_{S\text{-}Au} + d_{bulk} + d_{interface} = 0.19 \text{ nm} + (\cos(30^o) \times l_{S\text{-}C}) + 1.85 \text{ nm} \quad \text{(S8)}$$

$$d_{odd} = d_{S\text{-}Au} + d_{odd} + d_{interface} = 0.19 \text{ nm} + (\cos(30^o) \times l_{S\text{-}C}) + 0.55 \text{ nm} \quad \text{(S9)}$$

where $l_{S\text{-}C}$ is the length of the alkyl chain from the sulfur atom to the C atom indicated in the scheme for n_{odd} and n_{even} and calculated using a C-C bond length of 0.154 nm, S-C bond length of 0.181 nm, and ∠ C-C-C of 109.5°. The thicknesses of the interfacial CH_3 (n_{odd}) and CH_2CH_3 (n_{even}) layers are 0.55 nm and 1.85 nm, respectively,[25] and the Au-S layer thickness is 0.19 nm.[25-26] Inset: plot of the calculated d vs n. Lines are a guide to the eye. Fitting of the d–n data set yields an odd-even variation (Δ) of 0.2 Å for the ideal orientation of the chain termini in SAMs of n_{odd} and n_{even}.

Table S3. Statistical analysis (99% confidence level) of the $CH_3(CH_2)_nSAu$ SAM dielectric constant ε_{SAM} calculated from the capacitance.

n	$\bar{x}$	s	N	Tested Pairs	P-value	$t_{calculated}$	$t_{Student}$	df
6	2.05	0.07	16	n = 6/7	0.0025	3.316	2.763	28
7	1.92	0.14	14	n = 7/8	1.9×10^{-5}	5.100	2.756	29
8	2.12	0.09	17	n = 8/9	5.4×10^{-5}	4.593	2.724	35
9	1.99	0.09	20	n = 9/10	3.1×10^{-7}	6.229	2.715	37
10	2.19	0.11	19	n = 10/11	1.4×10^{-4}	4.364	2.75	30
11	2.04	0.07	13	n = 11/12	1.1×10^{-7}	7.153	2.771	27
12	2.24	0.08	16	n = 12/13	1.7×10^{-5}	5.262	2.779	26
13	2.11	0.05	12	n = 13/14	2.8×10^{-4}	5.063	3.055	12
14	2.29	0.11	10	n = 14/15	0.0084	2.815	2.744	31
15	2.18	0.10	23	n = 15/16	6.9×10^{-5}	4.480	2.715	37
16	2.34	0.11	16	n = 16/17	2.7×10^{-4}	4.065	2.728	34
17	2.19	0.11	20	n = 17/18	1×10^{-5}	5.263	2.744	31
18	2.38	0.10	13	n = 18/19	3×10^{-4}	4.248	2.807	23
19	2.24	0.07	12					

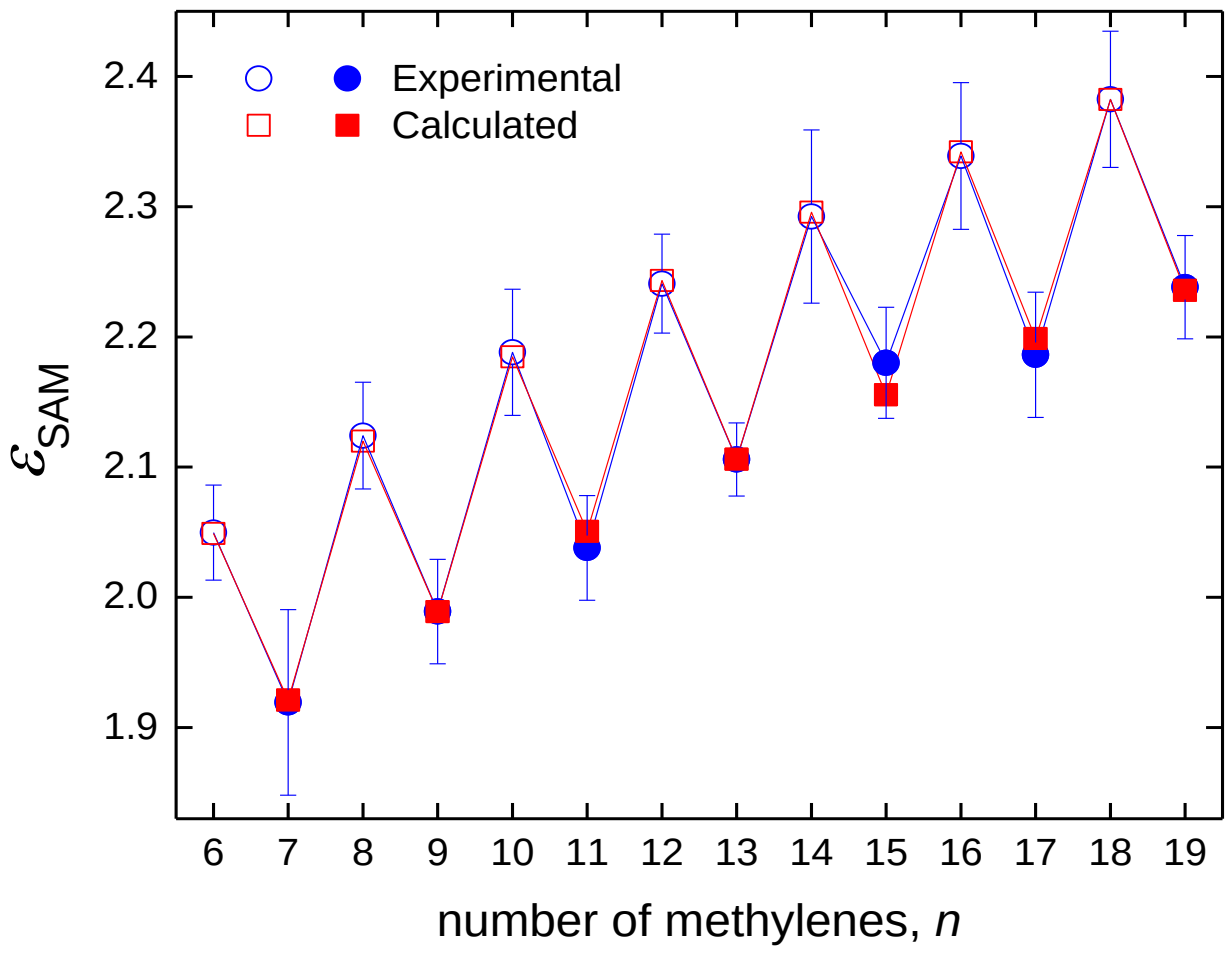

Figure S8. Fitting of the ε_{SAM}–n data set yields an odd-even variation (Δ) of 0.16. The values of a, b, c and Δ minimize the sum of the squared residuals (least-squares fit) between the experimental values of ε_{SAM} and the values calculated by the following set of second-order polynomial equations:

$$\varepsilon_n = \begin{cases} an^2 + bn + c & n_{even} \\ an^2 + bn + c - \Delta & n_{odd} \end{cases}$$

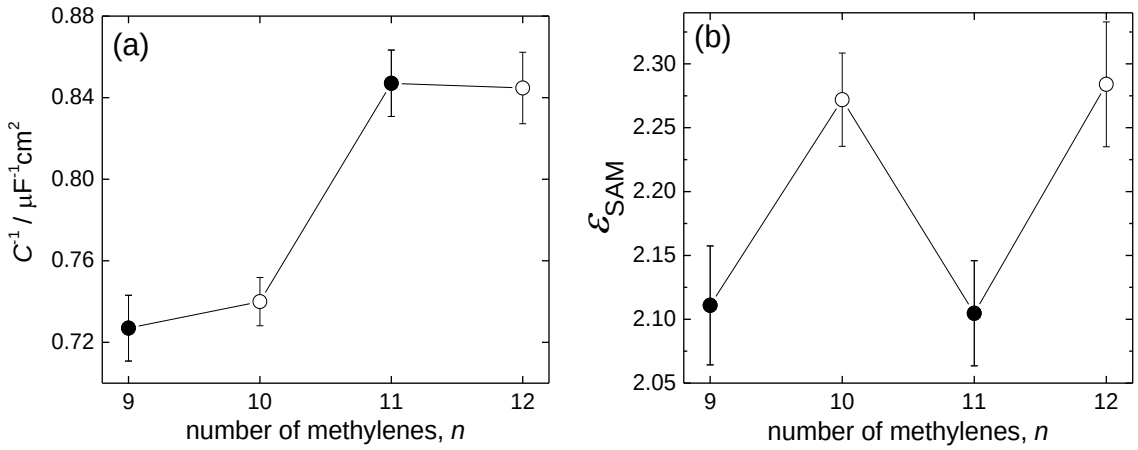

Figure S9. Reciprocal of the SAM capacitance C^{-1} and dielectric constant ε_{SAM} obtained in 1.0 M $NaCH_3SO_{4(aq)}$. The symbols and error bars represent the mean and 95% confidence interval of 8–10 different SAMs per *n*. Lines are a guide to the eye.

Calculation of the Dipole Moment of $CH_3SO_4^-$

The $CH_3SO_4^-$ dipole moment of 6 D was determined by a DFT calculation (Gaussian 16)[27] using the B3LYP method with a 6-311++G(d,p) basis set. The calculation included water as an implicit solvent.

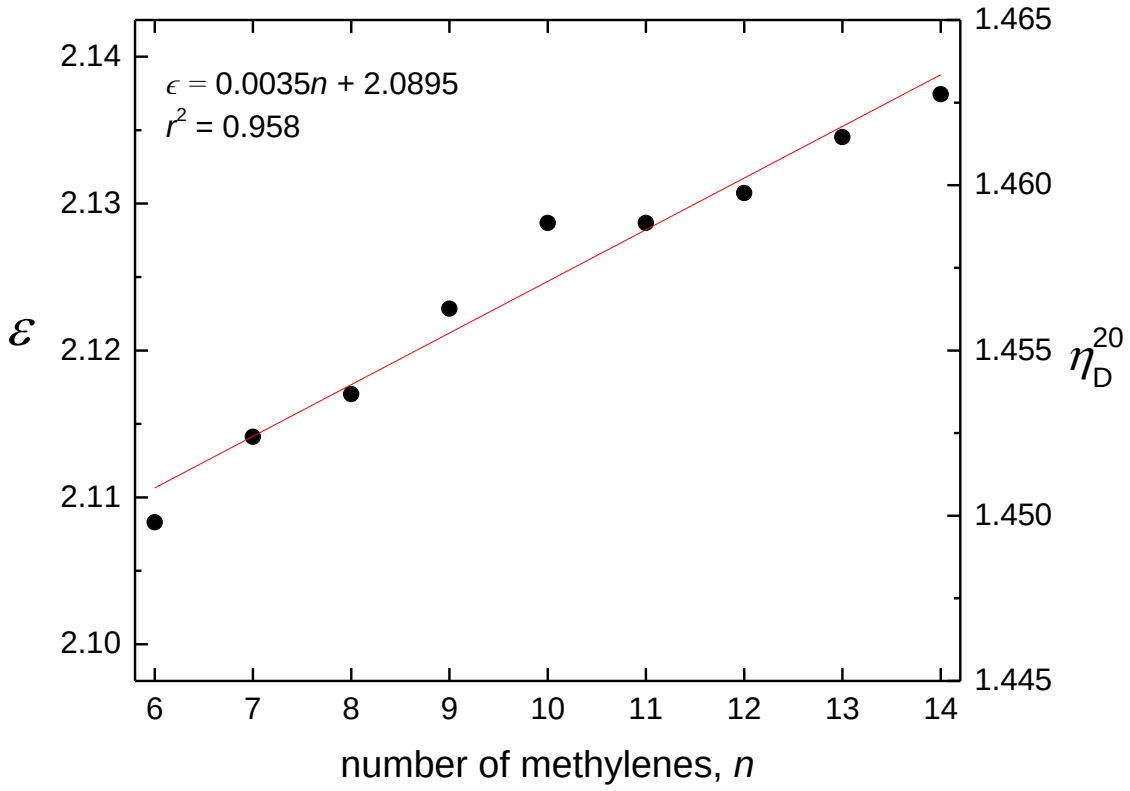

Figure S10. Literature values of the refractive index of liquid *n*-alkanethiols measured at 589.6 nm and 20 °C (η_D^{20}) (Sigma-Aldrich and ref [28]). Optical dielectric constant $\varepsilon = \eta^2 - k^2$, where η and k are the wavelength dependent refractive index and extinction coefficient. Assuming no absorption at the measurement wavelength (i.e., $k = 0$), $\varepsilon = \eta^2$. The red line is a linear regression of the ε data.

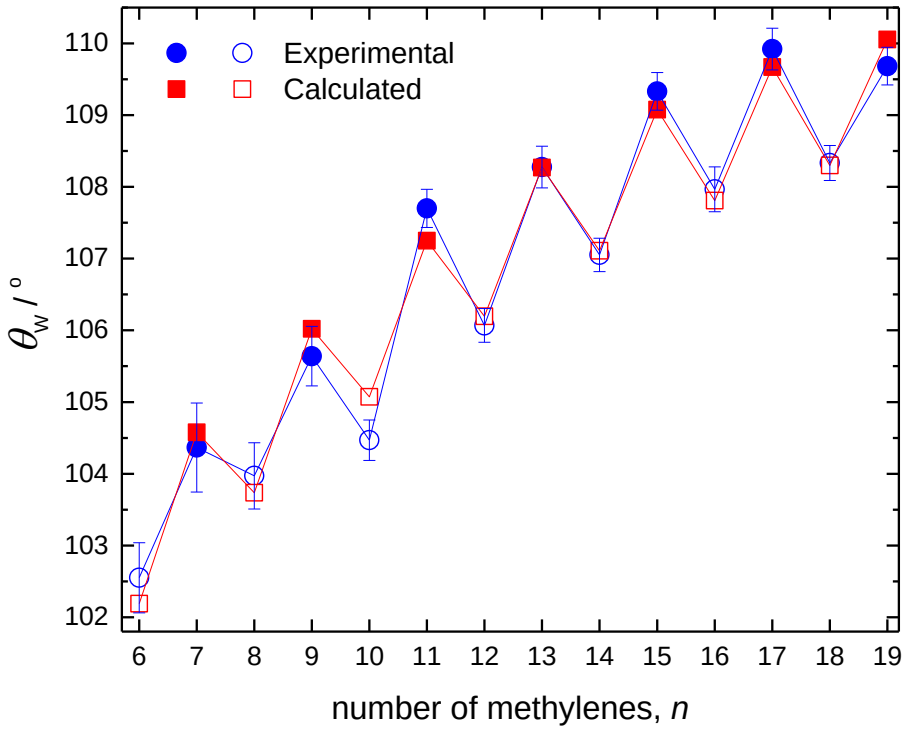

Figure S11. Fitting of the static contact angle of water (θ_w)–n data set yields an odd-even variation (Δ) of 1.6°. The values of a, b, c and Δ minimize the sum of the squared residuals (least-squares fit) between the experimental values of θ_w and the values calculated by the following set of second-order polynomial equations:

$$\theta_w = \begin{cases} an^2 + bn + c & n_{even} \\ an^2 + bn + c + \Delta & n_{odd} \end{cases}$$

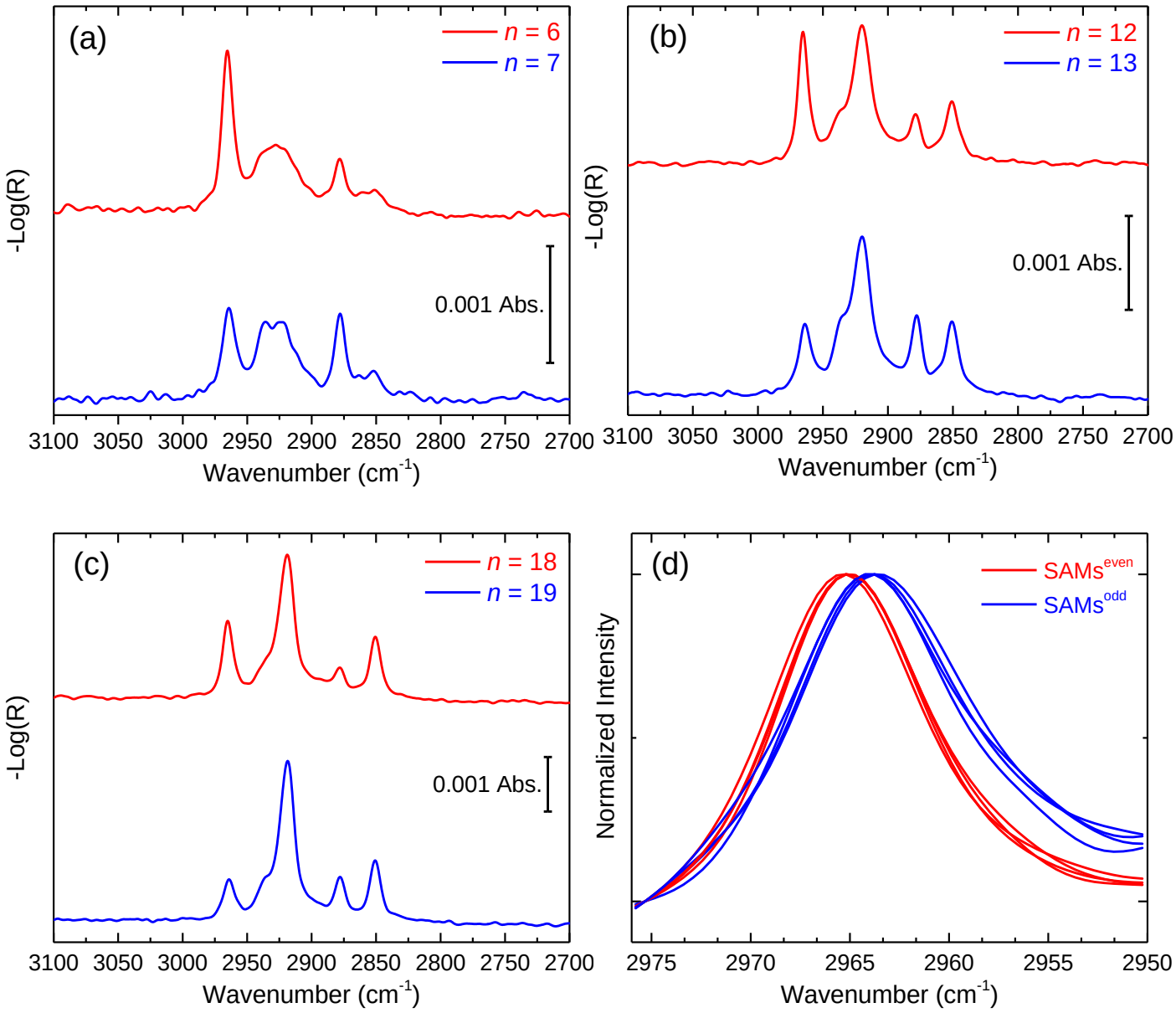

Figure S12. IRRAS spectra of selected chain lengths of $CH_3(CH_2)_nSAu$ SAMs: (a) n = 6 and 7, (b) n = 12 and 13, and (c) n = 18 and 19. (d) Comparison of υ_a (CH_3) of $SAMs^{odd}$ and $SAMs^{even}$ for n = 12–19. Spectra were recorded at room temperature with the *p*-polarized light incident at 80°.

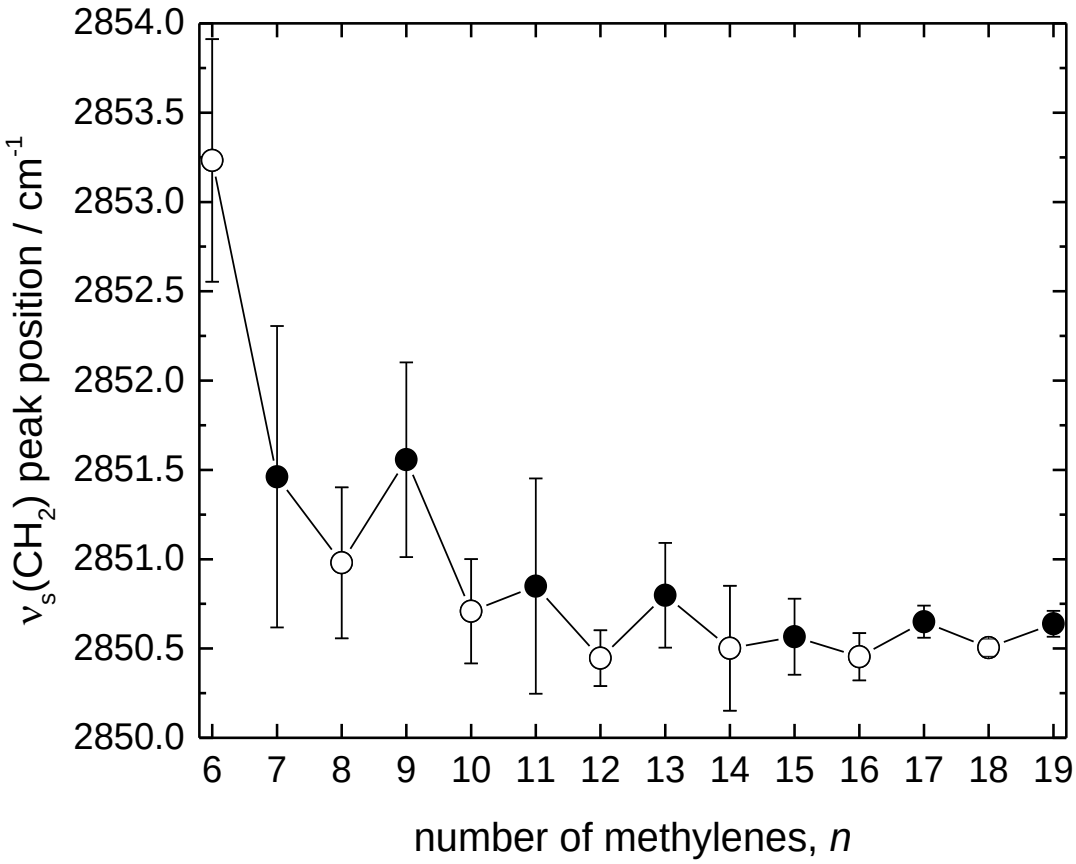

Figure S13. $\nu_s(CH_2)$ peak position as a function of *n*. Symbols and error bars represent the mean and 95% confidence interval of 5–12 independently prepared SAMs per *n*. Solid lines are a guide to the eye.

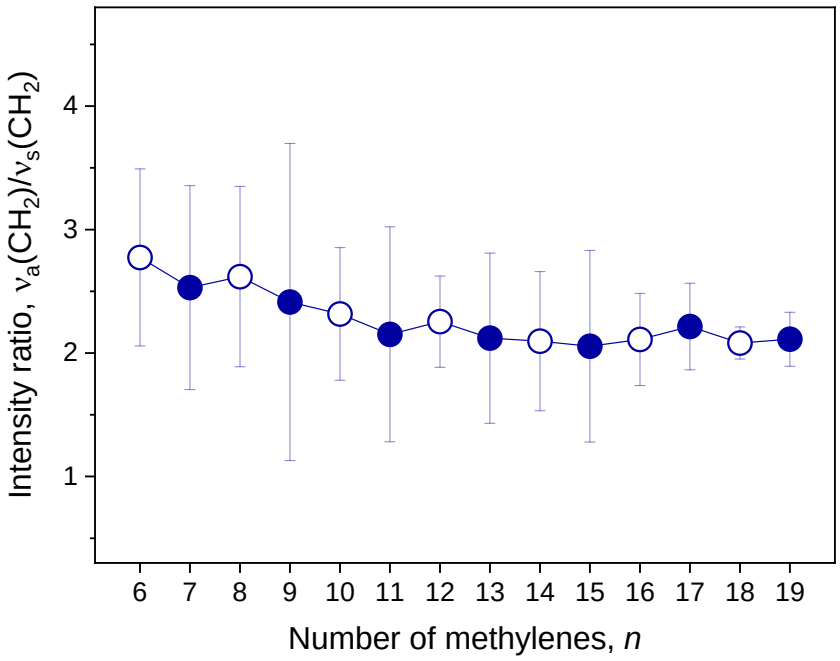

Figure S14. Ratio of the intensities of $\nu_a(CH_2)$ and $\nu_s(CH_2)$ as a function of *n*. Symbols and error bars represent the mean and 95% confidence interval of 5–12 independently prepared SAMs per *n*. Solid lines are a guide to the eye.

Estimation of the Refractive Index of a Functional Group

The refractive index η of a single molecule (e.g., $CH_3(CH_2)_4CH_3$) or molecular fragment (e.g., CH_2CH_3) can be estimated by separating the molecule into parts whose refractive indices are known, and the refractive index of the groups can be summed after scaling each with a weighting factor equal to the fraction ϕ of the molecule's volume that is occupied by that group:[29]

$$\eta = \phi_{CH2}\eta_{CH2} + \phi_{CH3}\eta_{CH3} \qquad \text{(S10)}$$

1. For example, assuming that the CH_2 and CH_3 groups occupy the same volume**,** the refractive index of $CH_3(CH_2)_4CH_3$ can be estimated using the relation:

$$\eta_{\text{hexane}} = 1/3\,\eta_{\text{CH3}} + 2/3\,\eta_{\text{CH2}} \qquad \text{(S11)}$$

Refractive index at 589 nm of CH_2 group = 1.471.[29]
Refractive index at 589 nm of CH_3 group = 1.183.[29]

$$\eta_{\text{hexane}} = 1/3(1.183) + 2/3(1.471) = 1.375$$

The refractive index of hexane measured at 589 nm and 20 ^{o}C is 1.375.[30]

2. In the same way, the refractive index and optical dielectric constant ε of the CH_2CH_3 fragment can be estimated using the relation:

$$\eta_{\text{ethyl}} = 0.5(1.183) + 0.5(1.471) = 1.327$$

$$\varepsilon_{\text{ethyl}} = (1.327)^2 = 1.7609$$

3. REFERENCES

1. Liu, Z. H.; Brown, N. M. D.; McKinley, A., Evaluation of the Growth Behaviour of Gold Film Surfaces Evaporation-Deposited on Mica under Different Conditions. *J. Phys.: Condens. Matter* **1997,** *9*, 59-71.

2. Mahmoodi, N.; Rushdi, A. I.; Bowen, J.; Sabouri, A.; Anthony, C. J.; Mendes, P. M.; Preece, J. A., Room Temperature Thermally Evaporated Thin Au film on Si Suitable for Application of Thiol Self-Assembled Monolayers in Micro/Nano-electro-mechanical-systems Sensors. *J. Vac. Sci. Technol. A* **2017,** *35*, 041514.

3. Itagaki, M.; Suzuki, S.; Shitanda, I.; Watanabe, K., Electrochemical Impedance and Complex Capacitance to Interpret Electrochemical Capacitor. *Electrochemistry (Tokyo, Jpn.)* **2007,** *75*, 649-655.

4. Góes, M. S.; Rahman, H.; Ryall, J.; Davis, J. J.; Bueno, P. R., A Dielectric Model of Self-Assembled Monolayer Interfaces by Capacitive Spectroscopy. *Langmuir* **2012,** *28*, 9689-9699.

5. Orazem, M. E.; Tribollet, B., *Electrochemical Impedance Spectroscopy*. John Wiley & Sons, Inc.: Hoboken, N.J., 2008.

6. Randriamahazaka, H.; Asaka, K., Electromechanical Analysis by Means of Complex Capacitance of Bucky-Gel Actuators Based on Single-Walled Carbon Nanotubes and an Ionic Liquid. *J. Phys. Chem. C* **2010,** *114*, 17982-17988.

7. Boubour, E.; Lennox, R. B., Insulating Properties of Self-Assembled Monolayers Monitored by Impedance Spectroscopy. *Langmuir* **2000,** *16*, 4222-4228.

8. Janek, R. P.; Fawcett, W. R.; Ulman, A., Impedance Spectroscopy of Self-Assembled Monolayers on Au(111): Evidence for Complex Double-Layer Structure in Aqueous NaClO4 at the Potential of Zero Charge. *J. Phys. Chem. B* **1997,** *101*, 8550-8558.

9. Wang, W.; Zhang, S.; Chinwangso, P.; Advincula, R. C.; Lee, T. R., Electric Potential Stability and Ionic Permeability of SAMs on Gold Derived from Bidentate and Tridentate Chelating Alkanethiols. *J. Phys. Chem. C* **2009,** *113*, 3717-3725.

10. Feng, Y.; Dionne, E. R.; Toader, V.; Beaudoin, G.; Badia, A., Odd–Even Effects in Electroactive Self-Assembled Monolayers Investigated by Electrochemical Surface Plasmon Resonance and Impedance Spectroscopy. *J. Phys. Chem. C* **2017,** *121*, 24626-24640.

11. Conway, B. E., Impedance Behavior of Electrochemical Supercapacitors and Porous Electrodes In *Impedance Spectroscopy Theory, Experiment and Application, Second Edition*, Barsoukov, E.; Macdonald, J. R., Eds. John Wiley & Sons: Hoboken, N.J., 2005.

12. Weiss, E. A.; Kaufman, G. K.; Kriebel, J. K.; Li, Z.; Schalek, R.; Whitesides, G. M., Si/SiO2-Templated Formation of Ultraflat Metal Surfaces on Glass, Polymer, and Solder Supports: Their Use as Substrates for Self-Assembled Monolayers. *Langmuir* **2007,** *23*, 9686-9694.

13. Fenter, P.; Eisenberger, P.; Liang, K. S., Chain-length Dependence of the Structures and Phases of $CH3(CH2)_{n-1}SH$ Self-Assembled on Au(111). *Phys. Rev. Lett.* **1993,** *70*, 2447-2450.

14. Poirier, G. E., Characterization of Organosulfur Molecular Monolayers on Au(111) using Scanning Tunneling Microscopy. *Chem. Rev.* **1997,** *97*, 1117–1127.

15. Delamarche, E.; Michel, B.; Gerber, C.; Anselmetti, D.; Guentherodt, H. J.; Wolf, H.; Ringsdorf, H., Real-Space Observation of Nanoscale Molecular Domains in Self-Assembled Monolayers. *Langmuir* **1994,** *10*, 2869-2871.

16. Dionne, E. R.; Ben Amara, F.; Badia, A., An Electrochemical Immittance Analysis of the Dielectric Properties of Self-Assembled Monolayers. *Can. J. Chem.* **2020**, doi 10.1139/cjc-2020-0005.

17. Protsailo, L. V.; Fawcett, W. R., Electrochemical Impedance Spectroscopy at Alkanethiol-Coated Gold in Propylene Carbonate. *Langmuir* **2002,** *18*, 8933-8941.

18. Douglass Jr, E. F.; Driscoll, P. F.; Liu, D.; Burnham, N. A.; Lambert, C. R.; McGimpsey, W. G., Effect of Electrode Roughness On the Capacitive Behavior of Self-Assembled Monolayers. *Anal. Chem.* **2008,** *80*, 7670-7677.

19. Sahalov, H.; O'Brien, B.; Stebe, K. J.; Hristova, K.; Searson, P. C., Influence of Applied Potential on the Impedance of Alkanethiol SAMs. *Langmuir* **2007,** *23*, 9681-9685.

20. Darwish, N.; Eggers, P. K.; Ciampi, S.; Zhang, Y.; Tong, Y.; Ye, S.; Paddon-Row, M. N.; Gooding, J. J., Reversible Potential-Induced Structural Changes of Alkanethiol Monolayers on Gold Surfaces. *Electrochem. Commun.* **2011,** *13*, 387-390.

21. Olivier, G. K.; Shin, D.; Frechette, J., Factors Governing the Reversible Change in Ionic Permeability of a Low-Density Monolayer. *J. Electroanal. Chem.* **2010,** *639*, 50-58.

22. Agonafer, D. D.; Chainani, E.; Oruc, M. E.; Lee, K. S.; Shannon, M. A., Study of Insulating Properties of Alkanethiol Self-Assembled Monolayers Formed Under Prolonged Incubation Using Electrochemical Impedance Spectroscopy. *J. Nanotechnol. Eng. Med.* **2013,** *3*, 031006-1.

23. Protsailo, L. V.; Fawcett, W. R., Studies of Electron Transfer Through Self-Assembled Monolayers Using Impedance Spectroscopy. *Electrochim. Acta* **2000,** *45*, 3497-3505.

24. Harris, D. C., *Quantitative Chemical Analysis*. 6th ed.; W. H. Freeman and Co: 2003.

25. Baghbanzadeh, M.; Simeone, F. C.; Bowers, C. M.; Liao, K.-C.; Thuo, M.; Baghbanzadeh, M.; Miller, M. S.; Carmichael, T. B.; Whitesides, G. M., Odd–Even Effects in Charge Transport across n-Alkanethiolate-Based SAMs. *J. Am. Chem. Soc.* **2014,** *136*, 16919-16925.

26. Shi, J.; Hong, B.; Parikh, A. N.; Collins, R. W.; Allara, D. L., Optical Characterization of Electronic Transitions Arising from the Au/S Interface of Self-Assembled n-Alkanethiolate Monolayers. *Chem. Phys. Lett.* **1995,** *246*, 90-94.

27. Frisch, M. J.; Trucks, G. W.; Schlegel, H. B.; Scuseria, G. E.; Robb, M. A.; Cheeseman, J. R.; Scalmani, G.; Barone, V.; Petersson, G. A.; Nakatsuji, H.; Li, X.; Caricato, M.; Marenich, A. V.; Bloino, J.; Janesko, B. G.; Gomperts, R.; Mennucci, B.; Hratchian, H. P.; Ortiz, J. V.; Izmaylov, A. F.; Sonnenberg, J. L.; Williams; Ding, F.; Lipparini, F.; Egidi, F.; Goings, J.; Peng, B.; Petrone, A.; Henderson, T.; Ranasinghe, D.; Zakrzewski, V. G.; Gao, J.; Rega, N.; Zheng, G.; Liang, W.; Hada, M.; Ehara, M.; Toyota, K.; Fukuda, R.; Hasegawa, J.; Ishida, M.; Nakajima, T.; Honda, Y.; Kitao, O.; Nakai, H.; Vreven, T.; Throssell, K.; Montgomery Jr., J. A.; Peralta, J. E.; Ogliaro, F.; Bearpark, M. J.; Heyd, J. J.; Brothers, E. N.; Kudin, K. N.; Staroverov, V. N.; Keith, T. A.; Kobayashi, R.; Normand, J.; Raghavachari, K.; Rendell, A. P.; Burant, J. C.; Iyengar, S. S.; Tomasi, J.; Cossi, M.; Millam, J. M.; Klene, M.; Adamo, C.; Cammi, R.; Ochterski, J. W.; Martin, R. L.; Morokuma, K.; Farkas, O.; Foresman, J. B.; Fox, D. J. *Gaussian 16 Rev. C.01*, Wallingford, CT, 2016.

28. *CRC Handbook of Chemistry and Physics*. 100th ed.; CRC Press: 2019.

29. Jung, L. S.; Campbell, C. T.; Chinowsky, T. M.; Mar, M. N.; Yee, S. S., Quantitative Interpretation of the Response of Surface Plasmon Resonance Sensors to Adsorbed Films. *Langmuir* **1998,** *14*, 5636-5648.

30. https://www.sigmaaldrich.com/technical-documents/articles/biology/hexane-center.html (accessed 03/2020).